RESEARCH ARTICLE OPEN ACCESS

Modeling MOG Antibody–Associated Disorder and Neuromyelitis Optica Spectrum Disorder in Animal Models

Visual System Manifestations

Jana Remlinger, PhD, Maud Bagnoud, PhD, Ivo Meli, MSc, Marine Massy, MSc, Robert Hoepner, MD, Christopher Linington, PhD, Andrew Chan, MD, Jeffrey L. Bennett, MD, Volker Enzmann, PhD, and Anke Salmen, MD

Correspondence
PD Dr. med. Salmen
anke.salmen@insel.ch

Neurol Neuroimmunol Neuroinflamm 2023;10:e200141. doi:10.1212/NXI.0000000000200141

Abstract

Background and Objectives

Mechanisms of visual impairment in aquaporin 4 antibody (AQP4-IgG) seropositive neuromyelitis optica spectrum disorder (NMOSD) and myelin oligodendrocyte glycoprotein antibody (MOG-IgG)–associated disorder (MOGAD) are incompletely understood. The respective impact of optic nerve demyelination and primary and secondary retinal neurodegeneration are yet to be investigated in animal models.

Methods

Active MOG_{35-55} experimental autoimmune encephalomyelitis (EAE) was induced in C57BL/6Jrj mice, and monoclonal MOG-IgG (8–18C5, murine), recombinant AQP4-IgG (rAb-53, human), or isotype-matched control IgG (Iso-IgG, human) was administered 10 days post-immunization. Mobility impairment was scored daily. Visual acuity by optomotor reflex and ganglion cell complex thickness (GCC, 3 innermost retinal layers) by optical coherence tomography (OCT) were longitudinally assessed. Histopathology of optic nerve and retina was investigated during presymptomatic, acute, and chronic disease phases for immune cells, demyelination, complement deposition, natural killer (NK) cell, AQP4, and astrocyte involvement, retinal ganglion cells (RGCs), and Müller cell activation. Groups were compared by nonparametric tests with a p value <0.05 indicating statistical significance.

Results

Visual acuity decreased from baseline to chronic phase in MOG-IgG (mean ± standard error of the mean: 0.54 ± 0.01 to 0.46 ± 0.02 cycles/degree, $p < 0.05$) and AQP4-IgG EAE (0.54 ± 0.01 to 0.43 ± 0.02, cycles/degree, $p < 0.05$). Immune cell infiltration of optic nerves started in presymptomatic AQP4-IgG, but not in MOG-IgG EAE (5.85 ± 2.26 vs 0.13 ± 0.10 macrophages/region of interest [ROI] and 1.88 ± 0.63 vs 0.15 ± 0.06 T cells/ROI, both $p < 0.05$). Few NK cells, no complement deposition, and stable glial fibrillary acid protein and AQP4 fluorescence intensity characterized all EAE optic nerves. Lower GCC thickness (Spearman correlation coefficient $r = -0.44$, $p < 0.05$) and RGC counts ($r = -0.47$, $p < 0.05$) correlated with higher mobility impairment. RGCs decreased from presymptomatic to chronic disease phase in MOG-IgG (1,705 ± 51 vs 1,412 ± 45, $p < 0.05$) and AQP4-IgG EAE (1,758 ± 14 vs 1,526 ± 48, $p < 0.01$). Müller cell activation was not observed in either model.

From the Department of Neurology (J.R., M.B., I.M., M.M., R.H., A.C., A.S.), Inselspital, Bern University Hospital and Department for BioMedical Research (DBMR), University of Bern, Switzerland; Graduate School for Cellular and Biomedical Sciences (J.R., M.M.), University of Bern, Switzerland; Institute of Infection (C.L.), Immunity and Inflammation, University of Glasgow, UK; Departments of Neurology and Ophthalmology (J.L.B.), Programs in Neuroscience and Immunology, University of Colorado Anschutz Medical Campus, Aurora; and Department of Ophthalmology (V.E.), Inselspital, Bern University Hospital and Department for BioMedical Research (DBMR), University of Bern, Switzerland.

Go to Neurology.org/NN for full disclosures. Funding information is provided at the end of the article.

The Article Processing Charge was funded by the authors.

Glossary

ADCC = antibody-dependent cellular cytotoxicity; **AQP4** = aquaporin 4; **BBB** = blood-brain barrier; **CCD** = charge-coupled device; **c/d** = cycles per degree; **CDC** = complement-dependent cytotoxicity; **dpi** = days postimmunization; **EAE** = experimental autoimmune encephalomyelitis; **GCC** = ganglion cell complex; **GFAP** = glial fibrillary acid protein; **IgG** = immunoglobulin G; **Iso** = isotype control; **LFB** = Luxol fast blue; **MOG** = myelin oligodendrocyte glycoprotein; **MOGAD** = myelin oligodendrocyte glycoprotein antibody–associated disorder; **MS** = multiple sclerosis; **NK** = natural killer; **NMOSD** = neuromyelitis optica spectrum disorder; **OCT** = optical coherence tomography; **OMR** = optomotor response; **ON** = optic neuritis; **PAS** = periodic acid–Schiff; **PFA** = paraformaldehyde; **rAb** = recombinant antibody; **RGCs** = retinal ganglion cells; **RNFL** = retinal nerve fiber layer; **ROI** = region of interest; **SEM** = standard error of mean.

Discussion

In a multimodal longitudinal characterization of visual outcome in animal models of MOGAD and NMOSD, differential retinal injury and optic nerve involvement were not conclusively clarified. Yet optic nerve inflammation was earlier in AQP4-IgG–associated pathophysiology. Retinal atrophy determined by GCC thickness (OCT) and RGC counts correlating with mobility impairment in the chronic phase of MOG-IgG and AQP4-IgG EAE may serve as a generalizable marker of neurodegeneration.

Optic neuritis (ON) is a common debilitating symptom of neuromyelitis optica spectrum disorder (NMOSD), myelin oligodendrocyte glycoprotein antibody (MOG-IgG)–associated disorder (MOGAD), and multiple sclerosis (MS). NMOSD and MOGAD often present with more severe vision loss when compared with MS.[1,2] Differences in underlying anterior visual pathway pathology might explain the differences in short-term and long-term visual outcome of these patients.[3] NMOSD and MOGAD are characterized by pathogenic antibodies against the water channel aquaporin 4 (AQP4-IgG) or the myelin protein MOG (MOG-IgG), respectively. In the CNS, AQP4-IgG targets astrocytes leading to astrocytosis and secondary demyelination.[4] However, retinal Müller cells likewise express high amounts of AQP4 suggesting an additional primary retina involvement. By contrast, MOG is expressed on myelin sheaths of optic nerve axons, and thus MOG-IgG binding induces primary demyelination.[4] Complement-dependent cytotoxicity (CDC) and antibody-dependent cellular cytotoxicity (ADCC) are involved in AQP4-targeted pathophysiology.[5,6] Natural killer (NK) cell–mediated cytotoxic activity has been assessed in vitro using CD107a surface mobilization with sera of patients with MOGAD.[7]

ON characteristics such as inflammation of the optic nerve with involvement of the optic nerve disc, thinning of distinct retinal layers, and decrease in visual acuity have recently been recapitulated in experimental animal models such as murine experimental autoimmune encephalomyelitis (EAE).[8-11] Primary retinal pathology was achieved only in naive animals by direct intravitreal transfer of AQP4-IgG.[12] EAE-induced neuroinflammation allows peripherally administered antibodies to pass the blood-brain barrier (BBB), bind target structures in optic nerve and retina, and contribute to lesion progression.[13,14] Easy accessibility of the visual system allows longitudinal observations of visual function and morphology that may mirror systemic neurodegeneration.[15] High-resolution images of the retina captured by optical coherence tomography (OCT) and behavioral assessment of visual acuity by optomotor response (OMR) allow noninvasive quantification of structural and functional changes.[9,10,15]

Despite well-characterized visual manifestations in EAE, investigations in modified EAE models using MOG-IgG and AQP4-IgG are scarce, and a direct comparison of visual system manifestations is lacking. Recently, we showed that MOG-IgG–augmented EAE affects visual acuity.[16] We comparatively investigated antibody-mediated murine experimental models of CNS demyelination for functional, morphologic, and histopathologic anterior visual pathway manifestations associated with antibodies against MOG or AQP4 or isotype control antibodies (Iso-IgG) at different stages of the disease.

Methods

Experimental Design

Anterior visual pathway pathology was comparatively investigated in MOG-IgG–augmented EAE, AQP4-IgG–augmented EAE, Iso-IgG–augmented EAE, and sham-immunized controls. In the same animals, as reported in our study of different spinal cord manifestations,[17] we evaluated functional visual outcome (OMR) and retina layer thickness (OCT) longitudinally at baseline and at acute and chronic disease phases. Histopathology was compared after preparation of optic nerves and eyes. Disease phases were defined according to clinical disease symptoms (i.e., mobility impairment). Animals not developing mobility impairment were excluded from analyses, except for animals assessed in presymptomatic disease phase.

Ethics Approval and Animal Husbandry

Governmental authorities of the Canton of Bern, Switzerland (BE134/16 and BE126/19) approved animal experiments. We complied with Animal Research: Reporting of In Vivo Experiments guidelines and Association for Research in

Figure 1 Overview of Visual Pathway Tissue Preparation and Histology

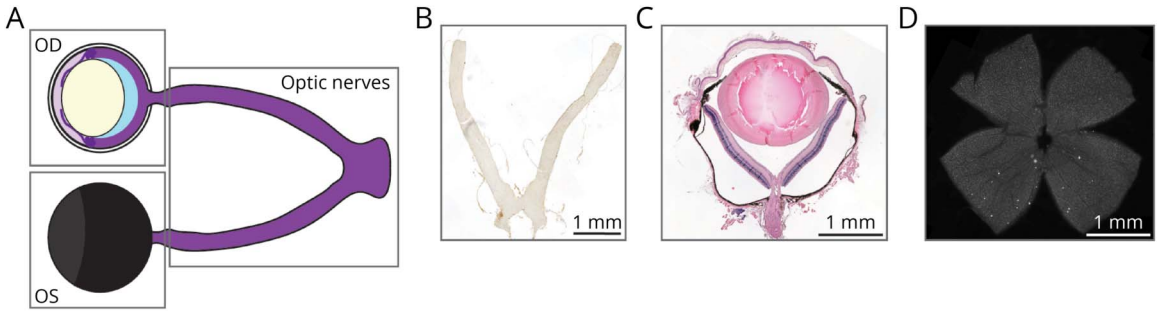

(A) Scheme of the anterior visual pathway including the right (OD), left eye (OS), and optic nerves with chiasm. Boxes indicate where the tissue was separated for histologic processing. (B) Representative image of a longitudinal optic nerve section (T cells, CD3 staining). Paraffin-embedded optic nerves including the chiasm were cut longitudinally into 5-µm thick sections. (C) Histologic representation of a transversely cut right eye including optic nerve head (hematoxylin-eosin staining). Paraffin-embedded bulbi were cut transversally into 7-µm thick sections including the optic nerve head. (D) Histologic representation of a retina flat mount prepared from fresh PFA-fixed left eyes (RGCs, Brn3a staining). PFA: paraformaldehyde; RGCs: retinal ganglion cells.

Vision and Ophthalmology Statement for the Use of Animals in Ophthalmic and Vision Research guidelines. Standardized animal husbandry and preexperimental procedures of female C57Bl/6JRj wild-type mice (Charles River Laboratories, Sulzfeld, Germany) were reported earlier.[17] Animal randomization according to weight and baseline visual acuity was performed for all experiments.

Induction of Antibody-Augmented MOG_{35-55} EAE

EAE induction and antibody administration were performed as previously reported.[17] In brief, EAE was induced with 100 µg of MOG peptide 35–55 (MOG_{35-55}) emulsified in complete Freund adjuvant under anesthesia required for OCT acquisition (see OCT). Pertussis toxin was injected between 0 and 2 days postimmunization (dpi). IV injection of 200 µg of monoclonal murine anti–MOG 8–18C5 IgG1 purified human monoclonal recombinant anti–AQP4 IgG1 (rAb-53),[18] or a purified human monoclonal recombinant IgG1 isotype control (rAb-2B4 directed against measles virus nucleocapsid protein)[19] was administered 10 dpi. Recombinant human antibodies were generated from paired heavy and light chain sequences previously identified and used in our previous work.[17-19] Animals were perfused, and the tissue was processed as reported.[17]

Assessment of Disease Course

Disease severity was assessed using a 10-point EAE scale according to mobility impairment (detailed in Ref. 16,17,20).

Optomotor Reflex Measurement

OMR was measured in vivo in nonanesthetized freely moving animals[21] to assess visual acuity at baseline (6 days–1 day before immunization), acute disease phase (14–16 dpi), and chronic disease phase (26–29 dpi), as previously described.[16] In brief, animals were placed on a platform in the center of 4 computer screens of a commercially available OMR system (OptoDrum; Striatech, Tübingen, Germany). Animal behavior (OMR) in response to a rotating black and white striped pattern (constant velocity of 6.1°/s and maximal contrast) was detected by a charge-coupled device (CCD) camera installed centrally above the platform and analyzed by the software provided. Stimulating pattern width (in cycles/degree [c/d]) for consecutive measurements was automatically adjusted in a staircase protocol. All stimuli were presented and assessed binocularly, and the threshold value per mouse was confirmed in repeated measurements.

Optical Coherence Tomography

Mice were anesthetized for OCT acquisition (50 mg/kg of ketamine; Ketanest, Zurich, Switzerland and 1 mg/kg of medetomidine; Dormitor, Provet AG, Lyssach, Switzerland). Mixed eye drops (Tropicamid 0.5%, phenylephrine HCl 2.5%, manufactured at Spitalpharmazie Inselgruppe, Bern, Switzerland) were applied to dilate the pupil, and the eye was hydrated (Methocel 2%, OmniVision, Puchheim, Germany). For image acquisition, mice were placed in front of the SD-OCT (Spectralis-OCT, Heidelberg Engineering, Heidelberg, Germany). With Heidelberg Eye Explorer (Heidelberg Engineering, version 1.10.2.0), fundus was imaged centered over the optic nerve head (infrared image) followed by Automatic Real-time Tracking OCT scan (31 scans) adjusted for small eyes (eTable 1, links.lww.com/NXI/A878). Follow-up measurements were performed using the respective setup of the software. Earliest 30 minutes after anesthesia induction, mice were awakened by an antagonist injection (1.25 mg/kg of atipamezol; Antisedan, Provet), hydrated with 300 µL of sodium chloride 0.9% solution and observed until fully recovered.

During postprocessing of OCT scans, retinal layers were segmented automatically in Heidelberg Spectralis system software (Heidelberg Eye Explorer, version 1.10.2.0; Heidelberg Engineering) and manually adjusted by an experienced annotator (J.R.). This segmentation software is especially reliable for the inner retinal layers that we focus on.[22] Ganglion cell complex (GCC) consisting of retinal nerve fiber layer (RNFL), ganglion cell layer, and inner plexiform layer was measured from segmentation border inner limiting membrane to inner nuclear layer (Figure 5A). Layer thickness values were extracted using a circular 1-, 2.22-,

Figure 2 Functional Visual Outcome of EAE With Administration of MOG-, AQP4- or Iso-IgG

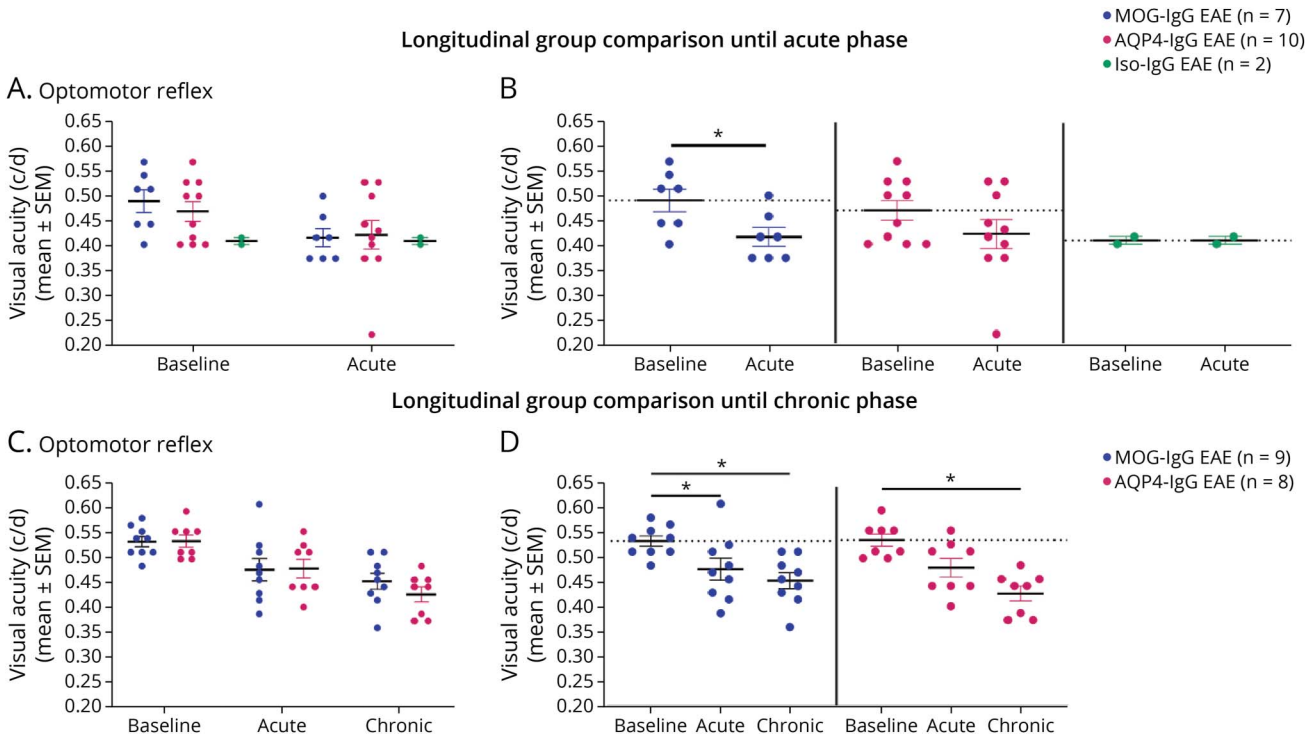

Visual acuity measured as optomotor reflex in response to a rotating grid pattern (c/d) at bl, ac disease phase, and chr disease phase. (A, B) Experiment with follow-up until acute disease phase in MOG-IgG (n = 7 paired observations), AQP4-IgG (n = 10 paired observations), and Iso-IgG EAE (n = 2 paired observations). Two independent experiments. (A) Disease model comparison at bl and ac disease phase: Kruskal-Wallis test. (B) Within-group comparisons: Wilcoxon signed-rank test. (C, D) Experiment with follow-up until chronic disease phase in MOG-IgG (n = 9 paired observations) and AQP4-IgG EAE (n = 8 paired observations). One experiment. (C) Disease model comparison at bl, ac disease phase, and chr disease phase: Mann-Whitney test. (D) Within-group comparisons: Friedman test. *$p < 0.05$. ac = acute; AQP4 = aquaporin 4; bl = baseline; chr = chronic; c/d = cycles per degree; DPI = days postimmunization; EAE = experimental autoimmune encephalomyelitis; MOG = myelin oligodendrocyte glycoprotein.

and 3.45-mm grid centered on the optic nerve head. The inner circle (1 mm in diameter) corresponding to the optic nerve head was excluded from the analysis and values from the 8 segments of the 2 outer circles were averaged.

To ensure quality, only scans with mean scan quality (signal-to-noise ratio) above 30 dB per eye and time point were evaluated. Scans displaying artefacts, shadows, or blurs hampered sublayer segmentation and were thus excluded (eTable 2, links.lww.com/NXI/A878).

Histology, Immunohistochemistry, and Immunofluorescence of Optic Nerve and Retina

Eyes and optic nerves including the chiasm were extracted after perfusion, fixed in 4% paraformaldehyde (PFA) for 24 hours, and embedded in paraffin (Figure 1A). Optic nerves were cut longitudinally into 5-µm thick sections (Figure 1, A and B) and bulbi into 7-µm thick sections that include the optic nerve head (Figure 1, A and C).

Luxol fast blue (LFB, Carl Roth, Arlesheim, Switzerland)/periodic acid Schiff (PAS, VWR International, Dietikon, Switzerland) staining revealed demyelination. Immunohistochemistry was used to stain macrophages (Mac3) and T cells (CD3), as described.[17]

By immunofluorescence staining, we visualized complement deposition with C5b-9 (mouse antihuman C5b-9, 10 µg/mL, Santa Cruz Biotechnology, Dallas, TX), NK cells (goat anti-mouse NKp46/NCR1, 20 µg/mL, Novus Biologicals, Centennial, CO) and NK cell activation with CD107a (rabbit antimouse LAMP1/CD107a, 2 µg/mL, Abcam, Cambridge, UK), astrocytes with glial fibrillary acidic protein (GFAP) (chicken anti-mouse GFAP, 21.6 µg/mL, Abcam), and AQP4 (rabbit antihuman AQP4, 4 µg/mL, Alomone Labs, Jerusalem, Israel) and Müller cells with glutamine synthetase (mouse antimouse GS, 3.3 µg/mL, Abcam). Stained tissue was imaged with a slide scanner (Pannoramic 250 Flash III, 3DHISTECH, Budapest, Hungary) or a Nikon microscope equipped with epifluorescence and CCD camera (Nikon Instruments Europe B.V., Egg, Switzerland). We evaluated images with CaseViewer (3DHISTECH) or ImageJ (National Institute of Health, NIH, Bethesda, MD).

Retinal Ganglion Cell Count on Whole Retina Flat Mounts

One eye per animal was fixed in 4% PFA for 24 hours and retinal flat mounts were prepared as described before[16] (Figure 1D). After immunofluorescence staining for retinal ganglion cells (RGCs, goat anti-Brn3a, 0.2 µg/mL, Santa Cruz Biotechnology, Dallas, TX), retinas were extended on a microscope slide with the RNFL facing upward and viewed on a

Figure 3 Quantification of Demyelination and Immune Cell Infiltration in the Optic Nerve

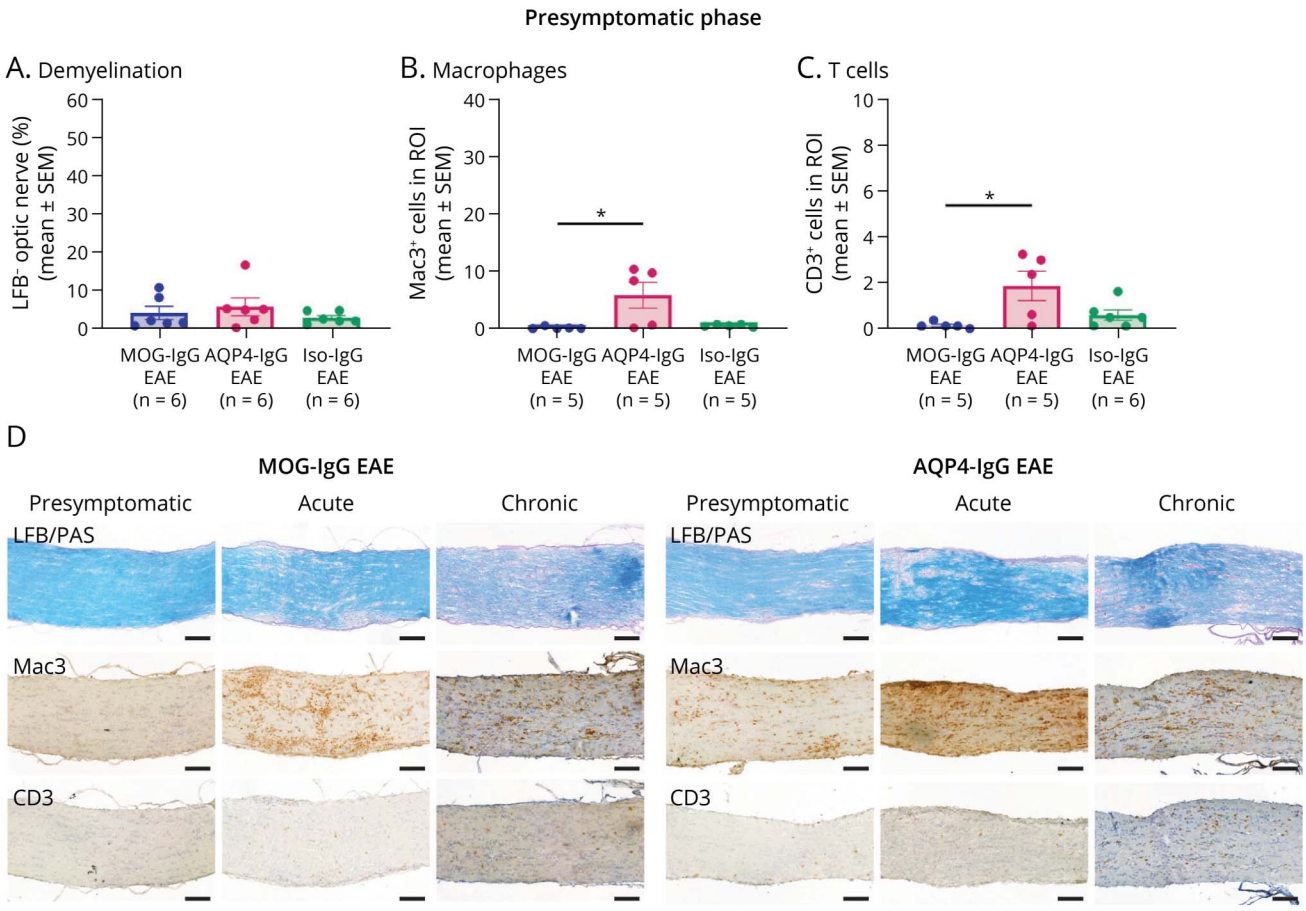

Disease model comparison at presymptomatic disease phase: Quantification of (A) percentage of demyelination after LFB/PAS staining, (B) macrophage infiltration after IHC for $Mac3^+$ cells, and (C) T-cell infiltration after IHC for $CD3^+$ cells. Presymptomatic: 1 experiment, acute: 2 independent experiments. Kruskal-Wallis test. $*p < 0.05$, $**p < 0.01$. (D) Histologic representation of LFB/PAS, Mac3, and CD3 IHC staining used for quantification at presymptomatic, acute disease phase, and chronic disease phase. Scale bars = 100 μm. AQP = aquaporin; EAE = experimental autoimmune encephalomyelitis; IgG = immunoglobulin G; IHC = immunohistochemistry; Iso = isotype control; LFB = Luxol fast blue; MOG = myelin oligodendrocyte glycoprotein; PAS = periodic acid–Schiff; ROI = region of interest.

Nikon microscope equipped with epifluorescence. Pictures were taken with a CCD camera (Nikon Instruments Europe B.V., Egg, Switzerland).

Quantification of Tissue Assessments

Evaluators were blinded for experimental groups in all quantifications. In longitudinal optic nerve sections, demyelinated area of the optic nerve was assessed with the color deconvolution plugin in ImageJ and expressed as percentage of the complete optic nerve section. Inflammation was assessed in retro-orbital, intermediate, and prechiasmatic thirds of the optic nerve. Considering Mac3, CD3, and LFB/PAS staining, each optic nerve pair was given 1 score per optic nerve section according to inflammation level: 0, no visible pathology; 1, diffuse inflammation; 2, diffuse inflammation and some lesions; and 3, clear lesion formation. Quantification of T cells, macrophages, NK cells, and $CD107a^+$ NK cells was manually performed with CaseViewer in 4 regions of interest (ROI, 100 × 100 μm) randomly distributed at regular intervals over the whole optic nerve tissue.

GFAP and AQP4 mean fluorescence intensity was measured by ImageJ within two 677-μm long optic nerve sections that showed inflammation representative for the whole optic nerve. RGCs were counted semiautomated in 4 ROI of 0.3 mm^2 around the optic nerve head using ImageJ.

Statistics

Statistical analysis was performed with Graph Pad 9 (Graph Pad Software Inc., San Diego, CA). Animal numbers are displayed in the graphs from pooled independent EAE experiments with the same experimental setup as indicated in the graph. Data are shown as mean plus/minus standard error of the mean (±SEM) or boxplots indicating median, minimum, and maximum. Nonparametric tests were used for group comparisons with a p value <0.05 indicating statistical significance and correction for multiple comparisons. Correlations were analyzed using Spearman rank correlation, determining Spearman rho (r) and the respective p value. For correlations of retinal assessments with mobility impairment, the mean clinical score represents the average of all scores per animal from the day of disease onset until the end of

Figure 4 Investigation of NK Cell Involvement to Assess ADCC in the Optic Nerve

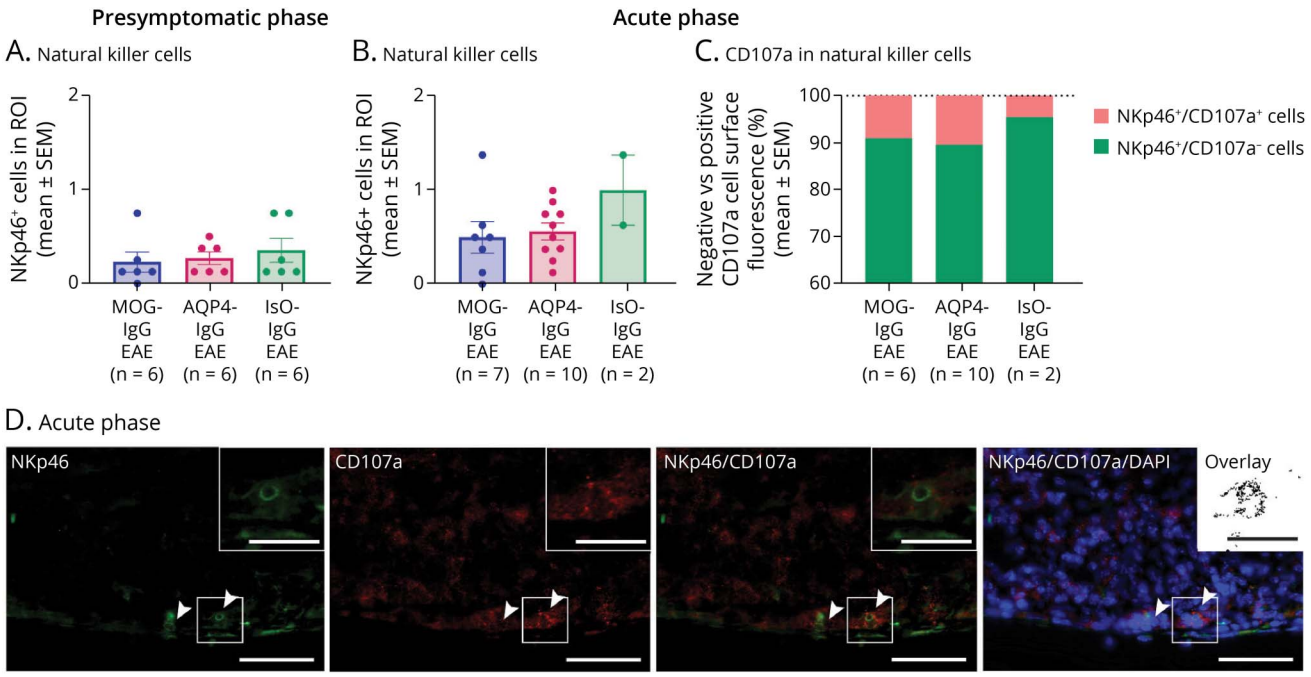

(A) Disease model comparison of number of NKp46-positive cells (NK cells) in optic nerves at presymptomatic disease phase. One experiment. Kruskal-Wallis test. p = ns. (B) Disease model comparison of number of NK cells (left) and (C) percentage of NK cells, negative (green) and positive (red) for CD107a cell surface staining (activated NK cells, right) in optic nerves at acute disease phase. Two independent experiments. Kruskal-Wallis test. p = ns. (D) Histologic representation of NKp46 and CD107a IF staining (DAPI counterstain) at acute disease (Iso-IgG EAE animal). Arrows indicate NKp46-positive cells. Insets show a higher magnification of boxed NKp46/CD107a double-positive cell with overlay analysis performed in image J. Scale bars = 50 and 20 μm (insets). ADCC = antibody-dependent cellular cytotoxicity; AQP = aquaporin; DAPI = 49,6-diamidino-2-phenylindole; EAE = experimental autoimmune encephalomyelitis; IgG = immunoglobulin G; IF = immunofluorescence; Iso = isotype control; MOG = myelin oligodendrocyte glycoprotein; ROI = region of interest.

experiment. Levels of significance are indicated as follows: ns = not significant; $^{*}p < 0.05$; $^{**}p < 0.01$; $^{***}p < 0.001$; and $^{****}p < 0.0001$. The Robust regression and Outlier removal test was performed for each dataset with Q = 1%.

Data Availability

Datasets supporting the conclusions of this article will be made available in the Bern Open Repository and Information System (BORIS doi: 10.48350/183215). Data on spinal cord manifestations of the animals included in this study are available in a preprint (http://dx.doi.org/10.2139/ssrn.4356442).

Results

Longitudinal Functional Visual Outcome

OMR responses as a proxy of visual acuity gradually decreased until chronic disease phase with significant differences from baseline to acute phase in MOG-IgG EAE (mean ± SEM: 0.54 ± 0.01 to 0.48 ± 0.02 c/d, $p = 0.0400$) and from baseline to chronic phase in MOG-IgG and AQP4-IgG EAE (mean ± SEM: MOG-IgG: 0.54 ± 0.01 to 0.46 ± 0.02 c/d, $p = 0.0140$; AQP4: 0.54 ± 0.01 to 0.43 ± 0.02 c/d, $p = 0.0373$; Figure 2, A–D).

A prior longitudinal experiment comparing all experimental groups (MOG-IgG, AQP4-IgG, Iso-IgG EAE, and sham immunization) using a previous OMR acquisition software did not show loss of visual acuity (eFigure 1, links.lww.com/NXI/A878).

Histologic Correlates of Inflammation and Demyelination in the Optic Nerve

Macrophage and T-cell infiltration into optic nerves appeared earlier in AQP4-IgG than in MOG-IgG EAE (Figure 3, A and B). Limited optic nerve demyelination was similar in presymptomatic MOG-IgG, AQP4-IgG, and Iso-IgG EAE (Figure 3C). Disease phase comparison in MOG-IgG and AQP4-IgG EAE corroborated this finding (eFigure 2C, links.lww.com/NXI/A878). Optic nerves of the few diseased Iso-IgG EAE animals at acute stage (n = 2) showed more demyelination and macrophage infiltration (eFigure 2A). No differences were detected for these features between Iso-IgG, MOG-IgG, and AQP4-IgG EAE at chronic disease phase except for lower demyelination in AQP4-IgG compared wih that in Iso-IgG EAE (eFigure 2B).

Localization of Inflammation and Demyelination and Inflammatory Patterns of the Optic Nerve

Longitudinal optic nerve sections show diffuse inflammation throughout the section in MOG-IgG, AQP4-IgG, and Iso-IgG EAE. Additional lesion formation was observed in some animals of all EAE groups (Figure 3D). Diffuse inflammatory and lesional patterns were evenly distributed over all 3 parts of the optic nerve (retro-orbital, intermediate, and prechiasmatic segments) in

Figure 5 Thickness of Ganglion Cell Complex of EAE With Administration of MOG-IgG, AQP4-IgG, or Iso-IgG and Sham-Immunized Controls

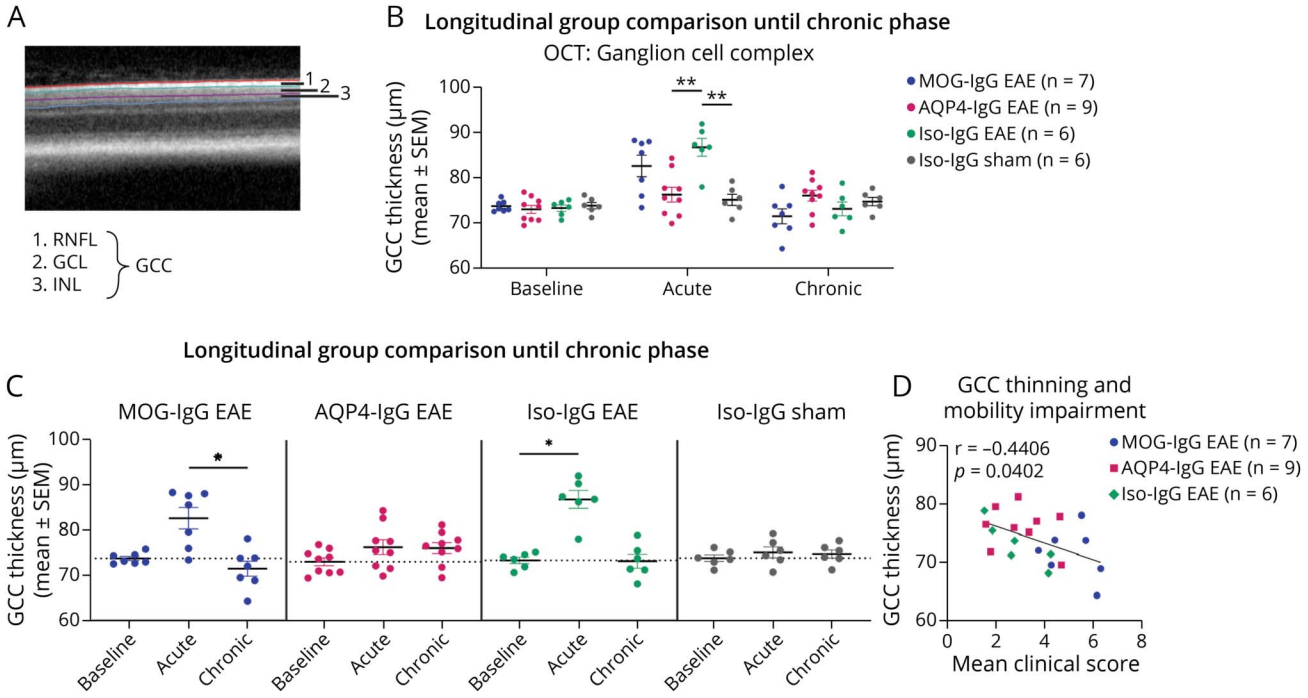

Ganglion cell complex thickness was evaluated through optical coherence tomography at bl, ac disease phase, and chr disease phase. (A) OCT retinal B-scan indicating GCC layer segmentation: GCC comprises RNFL, GCL, and IPL. (B, C) Experiment with follow-up until chronic disease phase in MOG-IgG EAE (n = 7 paired observations), AQP4-IgG EAE (n = 9 paired observations), Iso-IgG EAE (n = 6 paired observations), and sham-immunized controls (n = 6 paired observations). Two independent experiments. (B) Disease model comparison at bl, ac disease phase, and chr disease phase: Mann-Whitney test. (C) Within-group comparisons: Friedman test. *$p < 0.05$. (D) Correlation with mobility impairment. The mean clinical score reflects the average of all mobility impairment scores per animal from the day of disease onset until end of experiment. Spearman correlation coefficient r and p value indicated on graph. ac = acute; AQP4 = aquaporin 4; bl = baseline; chr = chronic; DPI = days postimmunization; EAE = experimental autoimmune encephalomyelitis; GCC = ganglion cell complex; GCL = ganglion cell layer; IPL = inner plexiform layer; Iso = isotype control; MOG = myelin oligodendrocyte glycoprotein; RNFL = retinal nerve fiber layer.

MOG-IgG, AQP4- IgG, and Iso-IgG EAE at all investigated time points (eFigure 2D-F, links.lww.com/NXI/A878). In MOG-IgG EAE, severity of inflammation increased in all 3 optic nerve parts from presymptomatic to acute disease, but only remained elevated until chronic disease phase in retro-orbital and prechiasmatic segments (eFigure 2G). In AQP4-IgG EAE, prechiasmatic inflammation score increased from presymptomatic to acute disease phase, while the inflammation score did not significantly change in the retro-orbital and intermediate optic nerve parts over the disease phases (eFigure 2G).

Natural Killer Cell Involvement and Complement Deposition in the Optic Nerve

At presymptomatic and acute disease stages, some NK cells were found in the optic nerves of all EAE groups (Figure 4, A, B and D), and few NK cells showed increased CD107a positivity at the cell surface (Figure 4C). No complement deposition was found in optic nerves at presymptomatic and acute stages.

GFAP and AQP4 Fluorescence Intensity in the Optic Nerve

Immunofluorescence intensity of GFAP and AQP4 within optic nerves was similar in all EAE groups at all disease phases (eFigure 3, links.lww.com/NXI/A878).

Longitudinal OCT Measurements of Ganglion Cell Complex Thickness

GCC thickness (Figure 5A) was stable from baseline to acute disease phase in MOG-IgG (mean ± SEM: 74.8 ± 1.25 to 77.8 ± 2.05 µm, $p = 0.1563$) and AQP4-IgG EAE (73.7 ± 0.6349 to 74.7 ± 1.19 µm, $p = 0.5742$; eFigure 4A, links.lww.com/NXI/A878). In Iso-IgG EAE, seeming increase of GCC thickness in acute disease phase (no statistics due to low numbers; eFigure 4A) was corroborated in a follow-up experiment (73.3 ± 0.70 to 86.7 ± 1.97 µm, $p = 0.0281$; Figure 5, B and C). GCC thickness decreased in MOG-IgG EAE from acute to chronic disease phase (82.6 ± 2.36 to 71.5 ± 1.66 µm, $p = 0.0226$; Figure 6C). This was not corroborated in a follow-up experiment (eFigure 4B). However, GCC at chronic disease stage was thinner with increased mobility impairment irrespective of the model system (Spearman coefficient $r = -0.4406$, $p = 0.0402$; Figure 5D, eFigure 4C).

Involvement of Retinal Ganglion Cells and Müller Cells

RGC counts were similar in all EAE groups at presymptomatic and acute disease phases (eFigure 5A, B, links.lww.com/NXI/A878). At chronic disease phase, less RGCs were found in MOG-IgG compared with those in AQP4-IgG EAE animals

Figure 6 Investigation of Retinal Ganglion Cells and Müller Cell Activation to Assess Retinal Involvement

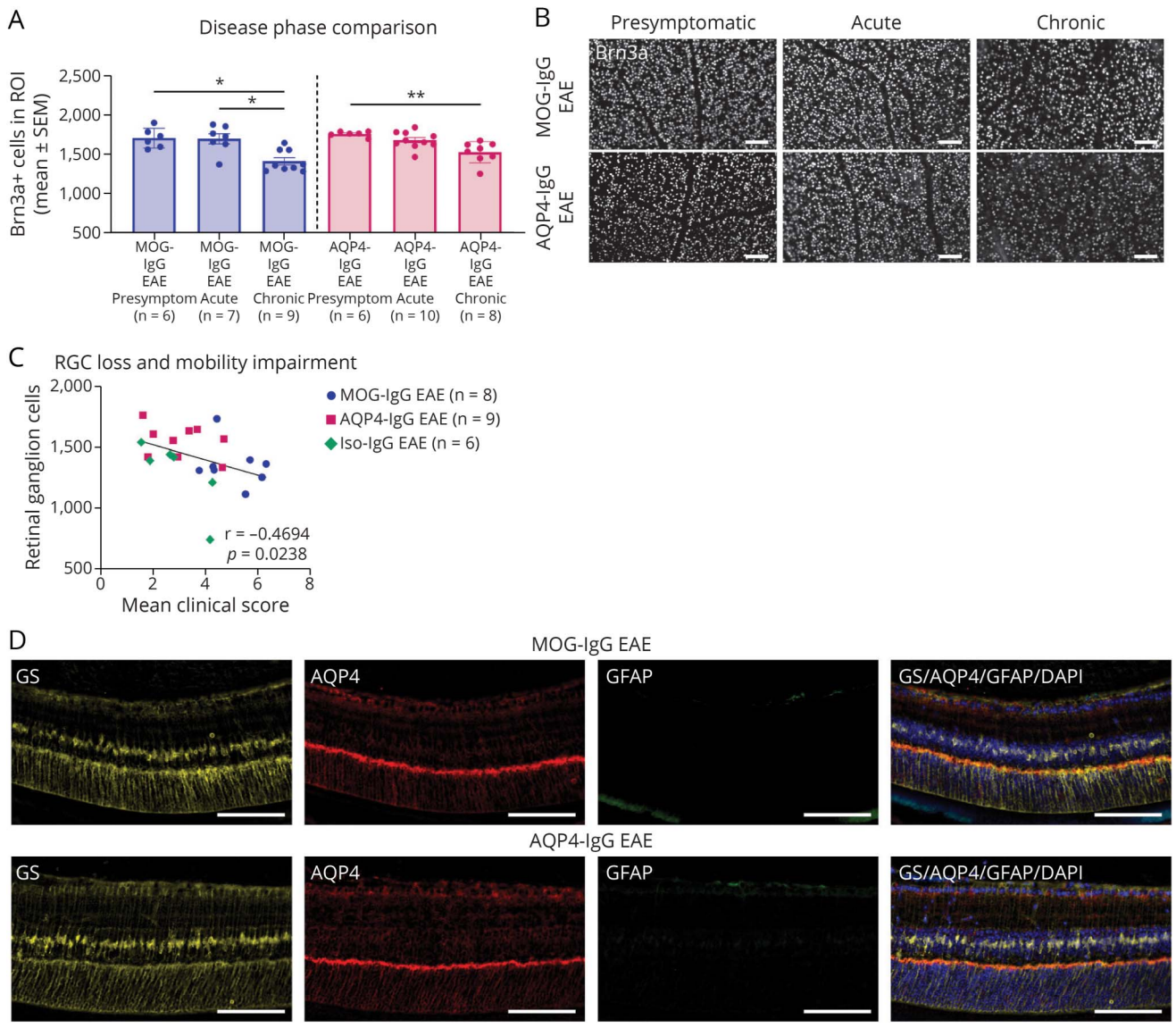

(A) Disease phase comparison of MOG-IgG EAE and AQP4-IgG EAE animals for RGC counts. Three independent experiments. Kruskal-Wallis test. *$p < 0.05$, **$p < 0.01$. (B) Histologic representation of Brn3a staining used for quantification at presymptomatic, acute, and chronic disease phases. Scale bars = 100 µm. (C) Correlation with mobility impairment. The mean clinical score reflects the average of all mobility impairment scores per animal from the day of disease onset until the end of experiment. Two independent experiments. Spearman correlation coefficient r and p value indicated on graph. (D) Histologic representation of IF staining of the retina showing Müller cells (GS), AQP4 and astrocytes/Müller cell activation (both GFAP). Scale bars = 100 µm. AQP = aquaporin; CFA = complete Freund adjuvant; EAE = experimental autoimmune encephalomyelitis; GFAP = glial fibrillary acidic protein; GS = glutamate synthetase; IF = immunofluorescence; IgG = immunoglobulin G; IHC = immunohistochemistry; Iso = isotype control; MOG = myelin oligodendrocyte glycoprotein; RGC = retinal ganglion cell; ROI = region of interest.

(eFigure 5C). This was not corroborated in a second experiment comparing only these 2 groups (eFigure 5D). Over the course of disease, RGC number decreased in MOG-IgG and AQP4-IgG EAE (Figure 6, A and B). At chronic disease phase, animals with an increased mobility impairment had lower RGC counts (MOG-IgG/AQP4-IgG/Iso-IgG: Spearman coefficient $r = -0.4694$, $p = 0.0238$; Figure 6C; MOG-IgG/AQP4-IgG: $r = -0.5236$, $p = 0.0328$; eFigure 5D). Müller cell activation assessed by GFAP immunofluorescence of GS-positive Müller cells or loss of AQP4 was not apparent in any EAE model at any investigated disease phase (Figure 6D).

Discussion

In this parallel experimental approach comparing different antibody-mediated murine models of CNS demyelination, we observed differences in visual function and optic nerve and retina histopathology between models and phases of the disease. Loss of visual acuity was apparent from acute stage onward in MOG-IgG EAE, whereas AQP4-IgG EAE showed significant loss of visual acuity only at chronic disease phase indicating differential time courses of functional visual impairment in our model systems. Assessment of visual acuity

has not only been a useful proxy for visual function dynamics in other MOG_{35-55} EAE animals[10,11] but also differentiated treatment effects in MOG_{35-55}[23] and MOG-IgG–augmented MOG_{35-55} EAE,[16] but not in AQP4-IgG–augmented MOG_{35-55} EAE. Likewise, although for both AQP4-IgG and MOG-IgG penetration into the CNS in comparable experimental settings has been demonstrated earlier,[24,25] a comparative approach analyzing the visual acuity after systemic MOG-IgG and AQP4-IgG administration in MOG_{35-55} EAE animals is lacking. However, in the human situation, high-contrast visual acuity seems more impaired in patients with NMOSD compared with patients with MOGAD and MS despite similar structural OCT features such as peripapillary RNFL and Ganglion cell - inner plexiform layer (GCIPL) thickness.[26,27]

Structural optic nerve changes in NMOSD and MOGAD are mainly analyzed by MRI because human tissue is rarely available. Yet some histopathologic hallmarks of inflammation such as immune cell infiltration, loss of myelin, and gliosis have been reported.[3,28] Optic nerves of all EAE animals studied here demonstrated a mixed pattern of diffuse inflammatory infiltration and demyelination with smaller and larger quantifiable lesional areas. No rostrocaudal distribution of lesion formation was observed in optic nerves. This observation is in contrast to our observations in spinal manifestations of different EAE models with antibody-dependent differential lesion localization and inflammation starting subpially, preferentially in ventrolateral localization for MOG-IgG and Iso-IgG EAE, and ventrally for AQP4-IgG EAE.[17] Overall lower presymptomatic inflammation scores increased over the course of disease in MOG-IgG EAE, but were already high in retro-orbital and intermediate AQP4-IgG EAE optic nerves, again reflecting differential optic nerve inflammation dynamics. Preferential sites of lesion localization in the optic nerve shown by others have required a different type of intervention. Perichiasmatic infusion of AQP4-IgG with human complement resulted in lesion formation preferentially at the infusion site.[29] Although systemic application mimics the suggested human pathophysiology with mostly peripheral antibody production more closely, it might not be sufficient to elicit differences in anterior visual pathway lesion localization. Studies focusing on specific lesion localization might thus benefit from local antibody application.

In AQP4-IgG EAE, immune cell infiltration into optic nerves appeared earlier and remained stable over the course of disease. Of interest, this is in line with earlier neuroinflammation in the spinal cord of AQP4-IgG EAE animals.[17] However, this was not reflected in the functional assessments with a significant loss of visual acuity only at chronic disease phase. The only other comparison of MOG-targeted and AQP4-targeted optic nerve pathology showed more severe morphological correlates of ON after disease induction by MOG-specific T-cell adoptive transfer compared with AQP4-specific T-cell adoptive transfer.[30] MOG-specific T-cell transfer resulted in more immune cell infiltration, reduced thickness of inner retinal layers (i.e., GCC), and more severe loss of RGCs compared with AQP4-specific T-cell injection. Such differences were not depicted in our comparison of the visual system using systemic MOG-IgG and AQP4-IgG administration on an MOG-peptide immunization background.

The latter surely creates a bias by not only causing BBB breakdown but inducing a predominantly T-cell driven EAE itself. Within an artificial model system, this first step is necessary to enable further antibody-driven processes within the CNS as shown in our analyses and as used in many other studies,[14,18,25] yet without distinct analyses of the visual system.

Our findings of more demyelination and immune cell infiltration into optic nerves at acute disease phase in Iso-IgG EAE were not reflected in functional assessments or RGC counts. The latter and the low incidence of EAE in this group and thus a low number of animals examined at acute stage questions the robustness of these results, which were not the primary focus of our work.

CDC and ADCC have been extensively studied as pathophysiologic mechanisms of AQP4-IgG–associated inflammation and tissue destruction in the brain and spinal cord,[5,6,31] but not optic nerves. In vitro experiments and animal models demonstrate AQP4 and MOG antibody binding to the antigen causes CDC in the presence of complement[18,32] and ADCC when NK cells or macrophages are present.[6,33,34] Pathology of human NMOSD and MOGAD lesions shows deposition of activated complement.[3,35] In the experimental animal models investigated in this study, both mechanisms were not sufficiently detectable in the optic nerves. The probably limited complement activity in the murine system might reduce the impact of CDC on histopathology in our setting. This might thus rather allow to study other antibody effector mechanisms such as ADCC. Neither bystander (for non-AQP4-IgG) nor direct (for AQP4-IgG) loss of AQP4 or astrocyte destruction was observed in inflammatory optic nerves of any EAE group compared with sham-immunized animals. Similarly, in a different experimental model for NMOSD using AQP4-specific T cells and NMOSD patient IgG (NMO-IgG) for disease induction, astrocyte-destructive lesions and AQP4 loss were essentially absent in optic nerves despite T-cell infiltration.[36] A model using adoptively transferred Th17-polarized AQP4-reactive T cells to induce EAE-like symptoms showed likewise preserved AQP4 despite T-cell infiltration and demyelination.[37] However, AQP4 and astrocyte immunofluorescence loss was apparent in the spinal cords of the AQP4-IgG EAE animals included in this study.[17] All these results emphasize the difficulty in modeling the full spectrum of human NMOSD and MOGAD pathology in any of the model systems presented. An increase in AQP4 immunofluorescence 60 days after MOG_{35-55} EAE induction and passive NMOSD patient–derived IgG (NMO-IgG) transfer at disease onset and repetitively thereafter to prevent disease remission might rather indicate long-term remodeling or reorganizing mechanisms under prolonged antibody challenge.[25] Loss of AQP4 immunofluorescence colocalizing with AQP4-IgG and GFAP loss

was shown after unilateral optic nerve subarachnoid injection of AQP4 IgG–positive serum.[38] With different administration routes for AQP4-IgG, only continuous perichiasmal infusion achieved ON compared with single perichiasmal or intravitreal injections.[29] These different reports may thus be associated with the mode of intervention, i.e., systemic vs local antibody administration. Distant interventions such as T-cell transfer or systemic antibody administration might not sufficiently expose consequences of MOG-IgG–associated optic nerve pathology and AQP4-IgG–associated optic nerve pathology compared with local application in the investigated tissue.

ON in patients with MOGAD and NMOSD is associated with retinal injury including thinning of the inner retinal layers (GCC)[2,39] and microcystic macular edema.[40] Likewise, OCT measurements in EAE animal models without antibody administration showed GCC thinning, which was associated with neuronal loss as measured by RGC counts.[41] In our comparison of MOG-IgG, AQP4-IgG, and Iso-IgG EAE, no clear reduction of GCC thickness was apparent over the course of disease as a group outcome. However, correlation analyses have revealed GCC thinning associated with overall disease severity. GCC swelling at acute disease phase in MOG-IgG and Iso-IgG EAE animals was observed, but not consistent between the experiments. Due to the lack of GCC thinning as a group outcome averaging both eyes per animal, stratification of the eyes according to the respective optic nerve inflammation intensity might be an interesting approach for future studies. Other OCT studies in MOG_{35-55} EAE animals have reported GCC swelling with a high variability shortly before acute disease phase.[8,9] Overall, GCC thickness seems prone to higher variability within experimental groups and between different studies.[9,10,15] This might explain the inconsistency seen in our study despite identical experimental procedures and suggest cautious interpretation of OCT measurements. This seems also in line with our histologic findings indicating high variability of optic nerve involvement irrespective of the model system. Other experimental models showed that acute swelling of GCC, in an AQP4-specific T-cell model returned to normal at chronic stage, whereas acute GCC swelling in mice that received MOG-specific T cells developed into progressive GCC thinning associated with loss of RGCs.[30] A connection of the GCC swelling and possibly more pronounced ON observed in Iso-IgG animals would have to be investigated further. In the human situation, lesions in patients with MOGAD with ON are more frequently retro-orbital relative to patients with NMOSD with prechiasmatic, chiasmatic, and optic tract lesions.[42] The lack of such localization preferences between our model systems might additionally explain the inconsistent presence of GCC swelling. Lack of GCC thinning in our study may also be attributed to the investigated time point because GCC thinning has been reported 8 weeks after MOG_{35-55}-immunization.[43] In human studies, chronic OCT outcomes reveal similar peripapillary RNFL and GCIPL (GCL+IPL) thicknesses in a comparison of patients with NMOSD, MOGAD, and MS,[26] whereas more severe peripapillary RNFL thickening in acute MOGAD ON may help to distinguish that observed in MS.[44]

In addition to GCC thickness, RGC counts reflect neurodegenerative involvement of the retina. In both MOG-IgG and AQP4-IgG EAE, RGC loss was apparent from presymptomatic to chronic disease phase reflecting, but not differentiating, neurodegeneration in the anterior visual pathway.

Correlation of lower RGC counts and thinner GCC with more severe mobility impairment reflects an important connection of visual system parameters with generalized neurodegeneration. Thus, OCT may represent a parallel approach to histology as a longitudinal, in vivo, paraclinical readout complementing the assessment of overall disability to detect neurodegeneration. As such, it is already used to monitor disease progression and mirror cortical atrophy in patients with demyelinating CNS disorders.[45,46]

A shortcoming of our systemically administered antibody model systems is the lacking discovery of a differential pathophysiology depending on antibody specificity, both in optic nerves and retina with comparable RGC loss. Müller cell pathology was not detected in our setup and thus did not reflect direct retinal effects of AQP4-IgG after systemic administration. Targeting of AQP4 by systemic administration of AQP4-specific T cells and NMO-IgG likewise showed only mild Müller cell pathology with loss of AQP4 side branches despite the presence of immune cells.[36] This might indicate difficulties with the systemic administration to induce an intraretinal pathology when compared with an intravitreal injection.[12] We are not aware of other experimental studies addressing Müller cell pathology after systemic administration of AQP4-IgG despite evidence from human postmortem tissue demonstrating AQP4 and GS loss in Müller cells.[28] Electrophysiologic assessments in patients with NMOSD showed a reduced b-wave amplitude when compared with patients with MS and healthy controls suggesting Müller cell dysfunction.[47] Microstructural changes in optic radiation of the Müller cell–rich foveal area and parafoveal thinning assessed by OCT may also be indicative of Müller cell pathology in patients with NMOSD.[48]

Other work in MOG_{35-55} EAE showed a decrease in AQP4 immunoreactivity at acute and chronic disease stages, especially in the GCC, compared with healthy control mice. GS immunofluorescence was weaker at acute disease stage.[8] Both events were subsequent to early astrogliosis in the GCC that might have induced Müller cell reactivity because they are in close contact through adherent junctions. Müller cells might also have reacted to optic nerve inflammation reaching the retina.[8] These features must rather reflect bystander Müller cell damage because no AQP4-specific intervention has been performed. AQP4 downregulation may also represent a protective mechanism against edema propagation in inflammatory models without an AQP4-targeted intervention.[8,49] In our study, GCC swelling was quite inconsistent and optic nerve pathology was milder compared with those observed in the aforementioned study. Gene expression analysis might expose more subtle Müller cell changes and thus complement further comparative investigations.

Yet the investigation of the anterior visual pathway after systemic antibody administration complements spinal cord findings and substantially contributes to disease understanding. Systemic administration may even more closely replicate extrathecal production of pathogenic antibodies in most patients with MOGAD and possibly exclusively in patients with NMOSD.[50] Although systemic antibody application performed on a background of MOG_{35-55} peptide immunization limits the direct comparison with the human diseases, many experimental studies using a similar approach have contributed immensely the understanding of pathophysiologic mechanisms.[14,18,25] Visual function dynamics have, to our knowledge, neither been assessed in AQP4-IgG EAE nor in a comparative approach of MOG-IgG and AQP-IgG EAE, so far. The only study comparing MOG-targeted optic nerve pathology and AQP4-targeted optic nerve pathology used antigen-specific T cells without antibody administration.[30] Additional studies using AQP4-IgG in combination with adoptive transfer of AQP4-specific T cells might complement our comparative approach.

Our parallel experimental investigations of the anterior visual pathway in EAE models of MOG-IgG–augmented EAE and AQP4-IgG–augmented EAE mimic aspects of the human diseases NMOSD and MOGAD. Yet a differential contribution of optic nerve and retinal injury in the distinct disease models could not be demonstrated. In line with our results in spinal cord histopathology, earlier inflammation occurs in the AQP4-IgG–associated model. Comparisons of visual outcomes and association with neurodegeneration and disease progression may be further studied in the described models. As an easily accessible paraclinical readout of pathologic retina changes, OCT allows the assessment of neurodegeneration in EAE, thus representing a promising outcome measure paralleling the human setup.

Acknowledgment

This work is part of a colead of Anke Salmen and Robert Hoepner of the research group Translational Neuroimmunology and Data Science.

Study Funding

Swiss Multiple Sclerosis Society Research Grant 2019/2020 Medical Faculty of the University of Bern.

Disclosure

J. Remlinger, M. Bagnoud, I. Meli, and M. Massy report no disclosures relevant to the manuscript. R. Hoepner received speaker/advisor honorary from Merck, Novartis, Roche, Biogen, Alexion, Sanofi, Janssen, Bristol-Myers Squibb, Teva/Mepha, and Almirall. He received research support within the past 5 years from Roche, Merck, Sanofi, Biogen, Chiesi, and Bristol-Myers Squibb. He also received research grants from the Swiss MS Society and is a member of the Advisory Board of the Swiss MS Society. He also serves as an associate editor for Journal of CNS disease. C. Linington reports no disclosures relevant to the manuscript. A. Chan has received speakers'/board honoraria from Actelion (Janssen/J&J), Almirall, Bayer, Biogen, Celgene (BMS), Genzyme, Merck KGaA (Darmstadt, Germany), Novartis, Roche, and Teva, all for hospital research funds. He received research support from Biogen, Genzyme, and UCB, the European Union, and the Swiss National Foundation. He serves as an associate editor of the European Journal of Neurology, on the editorial board for Clinical and Translational Neuroscience, and as a topic editor for the Journal of International Medical Research. J.L. Bennett was supported by grant NEI R01EY022936 from the National Eye Institute (NIH). V. Enzmann reports no disclosures relevant to the manuscript. A. Salmen received speaker honoraria and/or travel compensation for activities with Bristol Myers Squibb, CSL Behring, Novartis, and Roche and research support by the Baasch Medicus Foundation, the Medical Faculty of the University of Bern, and the Swiss MS Society. Go to Neurology.org/NN for full disclosures.

Publication History

Received by *Neurology: Neuroimmunology & Neuroinflammation* November 23, 2022. Accepted in final form May 15, 2023. Submitted and externally peer reviewed. The handling editor was Associate Editor Friedemann Paul, MD.

Appendix Authors

Name	Location	Contribution
Jana Remlinger, PhD	Department of Neurology, Inselspital, Bern University Hospital and Department for BioMedical Research (DBMR), University of Bern, Bern, Switzerland; Graduate School for Cellular and Biomedical Sciences, University of Bern, Bern, Switzerland	Drafting/revision of the article for content, including medical writing for content; major role in the acquisition of data; study concept or design; and analysis or interpretation of data
Maud Bagnoud, PhD	Department of Neurology, Inselspital, Bern University Hospital and Department for BioMedical Research (DBMR), University of Bern, Bern, Switzerland	Drafting/revision of the article for content, including medical writing for content; analysis or interpretation of data; and additional contributions: methodology and performance of experiments
Ivo Meli, MSc	Department of Neurology, Inselspital, Bern University Hospital and Department for BioMedical Research (DBMR), University of Bern, Bern, Switzerland	Drafting/revision of the article for content, including medical writing for content; analysis or interpretation of data; and additional contributions: methodology and performance of experiments
Marine Massy, MSc	Department of Neurology, Inselspital, Bern University Hospital and Department for BioMedical Research (DBMR), University of Bern, Bern, Switzerland; Graduate School for Cellular and Biomedical Sciences, University of Bern, Bern, Switzerland	Drafting/revision of the article for content, including medical writing for content; analysis or interpretation of data; and additional contributions: methodology and performance of experiments
Robert Hoepner, MD	Department of Neurology, Inselspital, Bern University Hospital and Department for BioMedical Research (DBMR), University of Bern, Bern, Switzerland	Drafting/revision of the article for content, including medical writing for content; analysis or interpretation of data; and additional contributions: methodology and statistics

Continued

Appendix *(continued)*

Name	Location	Contribution
Christopher Linington, PhD	Institute of Infection, Immunity and Inflammation, University of Glasgow, Glasgow, UK	Drafting/revision of the article for content, including medical writing for content; analysis or interpretation of data; and additional contributions: contribution of reagents/materials/analysis tools/infrastructure
Andrew Chan, MD	Department of Neurology, Inselspital, Bern University Hospital and Department for BioMedical Research (DBMR), University of Bern, Bern, Switzerland	Drafting/revision of the article for content, including medical writing for content; analysis or interpretation of data; and additional contributions: methodology and contribution of reagents/materials/analysis tools/infrastructure
Jeffrey L. Bennett, MD	Departments of Neurology and Ophthalmology, Programs in Neuroscience and Immunology, University of Colorado Anschutz Medical Campus, Aurora	Drafting/revision of the article for content, including medical writing for content; study concept or design; analysis or interpretation of data; and additional contributions: contribution of reagents/materials/analysis tools/infrastructure
Volker Enzmann, PhD	Department of Ophthalmology, Inselspital, Bern University Hospital and Department for BioMedical Research (DBMR), University of Bern, Bern, Switzerland	Drafting/revision of the article for content, including medical writing for content; study concept or design; analysis or interpretation of data; and additional contributions: methodology and contribution of reagents/materials/analysis tools/infrastructure
Anke Salmen, MD	Department of Neurology, Inselspital, Bern University Hospital and Department for BioMedical Research (DBMR), University of Bern, Bern, Switzerland	Drafting/revision of the article for content, including medical writing for content; major role in the acquisition of data; study concept or design; and analysis or interpretation of data

References

1. Jarius S, Wildemann B, Paul F. Neuromyelitis optica: clinical features, immunopathogenesis and treatment. *Clin Exp Immunol.* 2014;176(2):149-164. doi: 10.1111/cei.12271
2. Vicini R, Brugger D, Abegg M, Salmen A, Grabe HM. Differences in morphology and visual function of myelin oligodendrocyte glycoprotein antibody and multiple sclerosis associated optic neuritis. *J Neurol.* 2021;268(1):276-284. doi: 10.1007/s00415-020-10097-x
3. Höftberger R, Guo Y, Flanagan EP, et al. The pathology of central nervous system inflammatory demyelinating disease accompanying myelin oligodendrocyte glycoprotein autoantibody. *Acta Neuropathol.* 2020;139(5):875-892. doi: 10.1007/s00401-020-02132-y
4. Lopez JA, Denkova M, Ramanathan S, Dale RC, Brilot F. Pathogenesis of autoimmune demyelination: from multiple sclerosis to neuromyelitis optica spectrum disorders and myelin oligodendrocyte glycoprotein antibody-associated disease. *Clin Transl Immunol.* 2021;10(7):e1316. doi: 10.1002/cti2.1316
5. Ratelade J, Asavapanumas N, Ritchie AM, Wemlinger S, Bennett JL, Verkman AS. Involvement of antibody-dependent cell-mediated cytotoxicity in inflammatory demyelination in a mouse model of neuromyelitis optica. *Acta Neuropathol.* 2013;126(5):699-709. doi: 10.1007/s00401-013-1172-z
6. Ratelade J, Zhang H, Saadoun S, Bennett JL, Papadopoulos MC, Verkman AS. Neuromyelitis optica IgG and natural killer cells produce NMO lesions in mice without myelin loss. *Acta Neuropathol.* 2012;123(6):861-872. doi: 10.1007/s00401-012-0986-4
7. Brilot F, Dale RC, Selter RC, et al. Antibodies to native myelin oligodendrocyte glycoprotein in children with inflammatory demyelinating central nervous system disease. *Ann Neurol.* 2009;66(6):833-842. doi: 10.1002/ana.21916
8. Manogaran P, Samardzija M, Schad AN, et al. Retinal pathology in experimental optic neuritis is characterized by retrograde degeneration and gliosis. *Acta Neuropathol Commun.* 2019;7(1):116. doi: 10.1186/s40478-019-0768-5
9. Manogaran P, Walker-Egger C, Samardzija M, et al. Exploring experimental autoimmune optic neuritis using multimodal imaging. *Neuroimage.* 2018;175:327-339. doi: 10.1016/j.neuroimage.2018.04.004
10. Hecker C, Dietrich M, Issberner A, Hartung HP, Albrecht P. Comparison of different optomotor response readouts for visual testing in experimental autoimmune encephalomyelitis-optic neuritis. *J Neuroinflammation.* 2020;17(1):216. doi: 10.1186/s12974-020-01889-z
11. Larabee CM, Desai S, Agasing A, et al. Loss of Nrf2 exacerbates the visual deficits and optic neuritis elicited by experimental autoimmune encephalomyelitis. *Mol Vis.* 2016;22:1503-1513.
12. Felix CM, Levin MH, Verkman AS. Complement-independent retinal pathology produced by intravitreal injection of neuromyelitis optica immunoglobulin G. *J Neuroinflammation.* 2016;13(1):275. doi: 10.1186/s12974-016-0746-9
13. Linington C, Bradl M, Lassmann H, Brunner C, Vass K. Augmentation of demyelination in rat acute allergic encephalomyelitis by circulating mouse monoclonal antibodies directed against a myelin/oligodendrocyte glycoprotein. *Am J Pathol.* 1988;130(3):443-454.
14. Kinoshita M, Nakatsuji Y, Kimura T, et al. Neuromyelitis optica: passive transfer to rats by human immunoglobulin. *Biochem Biophys Res Commun.* 2009;386(4):623-627. doi: 10.1016/j.bbrc.2009.06.085
15. Dietrich M, Hecker C, Hilla A, et al. Using optical coherence tomography and optokinetic response as structural and functional visual system readouts in mice and rats. *J Vis Exp.* 2019;10:143. doi: 10.3791/58571
16. Remlinger J, Madarasz A, Guse K, et al. Antineonatal fc receptor antibody treatment ameliorates MOG-IgG-associated experimental autoimmune encephalomyelitis. *Neurol Neuroimmunol Neuroinflamm.* 2022;9(2):e1134. doi: 10.1212/NXI.0000000000001134
17. Remlinger J, Bagnoud M, Meli I, et al. Modelling MOG antibody-associated disorder and neuromyelitis optica spectrum disorder in animal models: spinal cord manifestations. Preprint available at http://dx.doi.org/10.2139/ssrn.4356442
18. Bennett JL, Lam C, Kalluri SR, et al. Intrathecal pathogenic anti-aquaporin antibodies in early neuromyelitis optica. *Ann Neurol.* 2009;66(5):617-629. doi: 10.1002/ana.21802
19. Burgoon MP, Williamson RA, Owens GP, et al. Cloning the antibody response in humans with inflammatory CNS disease: isolation of measles virus-specific antibodies from phage display libraries of a subacute sclerosing panencephalitis brain. *J Neuroimmunol.* 1999;94(1):204-211. doi: 10.1016/S0165-5728(98)00243-4
20. Bagnoud M, Briner M, Remlinger J, et al. c-Jun N-terminal kinase as a therapeutic target in experimental autoimmune encephalomyelitis. *Cells.* 2020;9(10):2154. doi: 10.3390/cells9102154
21. Prusky GT, West PWR, Douglas RM. Behavioral assessment of visual acuity in mice and rats. *Vis Res.* 2000;40(16):2201-2209. doi: 10.1016/S0042-6989(00)00081-X
22. Dysli C, Enzmann V, Sznitman R, Zinkernagel MS. Quantitative analysis of mouse retinal layers using automated segmentation of spectral domain optical coherence tomography images. *Transl Vis Sci Technol.* 2015;4(4):9. doi: 10.1167/tvst.4.4.9
23. Khan RS, Baumann B, Dine K, et al. Dexras1 deletion and iron chelation promote neuroprotection in experimental optic neuritis. *Sci Rep.* 2019;9(1):11664. doi: 10.1038/s41598-019-48087-3
24. Challa DK, Bussmeyer U, Khan T, et al. Autoantibody depletion ameliorates disease in murine experimental autoimmune encephalomyelitis. *Mabs.* 2013;5(5):655-659. doi: 10.4161/mabs.25439
25. Saini H, Rifkin R, Gorelik M, et al. Passively transferred human NMO-IgG exacerbates demyelination in mouse experimental autoimmune encephalomyelitis. *BMC Neurol.* 2013;13:104. doi: 10.1186/1471-2377-13-104
26. Gigengack NK, Oertel FC, Motamedi S, et al. Structure-function correlates of vision loss in neuromyelitis optica spectrum disorders. *Sci Rep.* 2022;12(1):17545. doi: 10.1038/s41598-022-19848-4
27. Sotirchos ES, Filippatou A, Fitzgerald KC, et al. Aquaporin-4 IgG seropositivity is associated with worse visual outcomes after optic neuritis than MOG-IgG seropositivity and multiple sclerosis, independent of macular ganglion cell layer thinning. *Mult Scler.* 2020;26(11):1360-1371. doi: 10.1177/1352458519864928
28. Hokari M, Yokoseki A, Arakawa M, et al. Clinicopathological features in anterior visual pathway in neuromyelitis optica. *Ann Neurol.* 2016;79(4):605-624. doi: 10.1002/ana.24608
29. Asavapanumas N, Ratelade J, Papadopoulos MC, Bennett JL, Levin MH, Verkman AS. Experimental mouse model of optic neuritis with inflammatory demyelination produced by passive transfer of neuromyelitis optica-immunoglobulin G. *J Neuroinflammation.* 2014;11(1):16. doi: 10.1186/1742-2094-11-16
30. Sagan SA, Winger RC, Cruz-Herranz A, et al. Tolerance checkpoint bypass permits emergence of pathogenic T cells to neuromyelitis optica autoantigen aquaporin-4. *Proc Natl Acad Sci.* 2016;113(51):14781-14786. doi: 10.1073/pnas.1617859114
31. Soltys J, Liu Y, Ritchie A, et al. Membrane assembly of aquaporin-4 autoantibodies regulates classical complement activation in neuromyelitis optica. *J Clin Invest.* 2019;129(5):2000-2013. doi: 10.1172/JCI122942
32. Spadaro M, Winklmeier S, Beltran E, et al. Pathogenicity of human antibodies against myelin oligodendrocyte glycoprotein. *Ann Neurol.* 2018;84(2):315-328. doi: 10.1002/ana.25291
33. Vincent T, Saikali P, Cayrol R, et al. Functional consequences of neuromyelitis optica-IgG astrocyte interactions on blood-brain barrier permeability and granulocyte recruitment. *J Immunol.* 2008;181(8):5730-5737. doi: 10.4049/jimmunol.181.8.5730
34. Vass K, Heininger K, Schäfer B, Linington C, Lassmann H. Interferon-γ potentiates antibody-mediated demyelination in vivo. *Ann Neurol.* 1992;32(2):198-206.

35. Lucchinetti CF, Mandler RN, McGavern D, et al. A role for humoral mechanisms in the pathogenesis of Devic's neuromyelitis optica. *Brain.* 2002;125(7):1450-1461. doi: 10.1093/brain/awf151
36. Zeka B, Hastermann M, Kaufmann N, et al. Aquaporin 4-specific T cells and NMO-IgG cause primary retinal damage in experimental NMO/SD. *Acta Neuropathol Commun.* 2016;4(1):82. doi: 10.1186/s40478-016-0355-y
37. Jones MV, Huang H, Calabresi PA, Levy M. Pathogenic aquaporin-4 reactive T cells are sufficient to induce mouse model of neuromyelitis optica. *Acta Neuropathol Commun.* 2015;3(1):28. doi: 10.1186/s40478-015-0207-1
38. Zhang Y, Bao Y, Qiu W, et al. Structural and visual functional deficits in a rat model of neuromyelitis optica spectrum disorders related optic neuritis. *Exp Eye Res.* 2018;175: 124-132. doi: 10.1016/j.exer.2018.06.011
39. Bennett JL, de Seze J, Lana-Peixoto M, et al. Neuromyelitis optica and multiple sclerosis: seeing differences through optical coherence tomography. *Mult Scler.* 2015; 21(6):678-688. doi: 10.1177/1352458514567216
40. Abegg M, Dysli M, Wolf S, Kowal J, Dufour P, Zinkernagel M. Microcystic macular edema: retrograde maculopathy caused by optic neuropathy. *Ophthalmol.* 2014; 121(1):142-149. doi: 10.1016/j.ophtha.2013.08.045
41. Cruz-Herranz A, Dietrich M, Hilla AM, et al. Monitoring retinal changes with optical coherence tomography predicts neuronal loss in experimental autoimmune encephalomyelitis. *J Neuroinflammation.* 2019;16(1):203. doi:10.1186/s12974-019-1583-4
42. Ramanathan S, Prelog K, Barnes EH, et al. Radiological differentiation of optic neuritis with myelin oligodendrocyte glycoprotein antibodies, aquaporin-4 antibodies, and multiple sclerosis. *Mult Scler.* 2016;22(4):470-482. doi: 10.1177/1352458515593406
43. Nishioka C, Liang HF, Barsamian B, Sun SW. Sequential phases of RGC axonal and somatic injury in EAE mice examined using DTI and OCT. *Mult Scler Relat Disord.* 2019;27:315-323. doi: 10.1016/j.msard.2018.11.010
44. Chen JJ, Sotirchos ES, Henderson AD, et al. OCT retinal nerve fiber layer thickness differentiates acute optic neuritis from MOG antibody-associated disease and Multiple Sclerosis: RNFL thickening in acute optic neuritis from MOGAD vs MS. *Mult Scler Relat Disord.* 2022;58:103525. doi: 10.1016/j.msard.2022.103525
45. Oertel FC, Zimmermann H, Paul F, Brandt AU. Optical coherence tomography in neuromyelitis optica spectrum disorders: potential advantages for individualized monitoring of progression and therapy. *EPMA J.* 2018;9(1):21-33. doi: 10.1007/s13167-017-0123-5
46. Rothman A, Murphy OC, Fitzgerald KC, et al. Retinal measurements predict 10-year disability in multiple sclerosis. *Ann Clin Translational Neurol.* 2019;6(2):222-232. doi: 10.1002/acn3.674
47. You Y, Zhu L, Zhang T, et al. Evidence of Müller glial dysfunction in patients with aquaporin-4 immunoglobulin G–positive neuromyelitis optica spectrum disorder. *Ophthalmology.* 2019;126(6):801-810. doi: 10.1016/j.ophtha.2019.01.016
48. Oertel FC, Kuchling J, Zimmermann H, et al. Microstructural visual system changes in AQP4-antibody–seropositive NMOSD. *Neurol Neuroimmunol Neuroinflamm.* 2017; 4(3):e334. doi: 10.1212/NXI.0000000000000334
49. Sun M-C, Honey CR, Berk C, Wong NL, Tsui JK. Regulation of aquaporin-4 in a traumatic brain injury model in rats. *J Neurosurg.* 2003;98(3):565-569. doi: 10.3171/jns.2003.98.3.0565
50. Akaishi T, Takahashi T, Misu T, et al. Difference in the source of anti-AQP4-IgG and anti-MOG-IgG antibodies in CSF in patients with neuromyelitis optica spectrum disorder. *Neurology.* 2021;97(1):e1. doi: 10.1212/WNL.0000000000012175

Modeling MOG Antibody–Associated Disorder and Neuromyelitis Optica Spectrum Disorder in Animal Models: Visual System Manifestations

Jana Remlinger, Maud Bagnoud, Ivo Meli, et al.

Neurol Neuroimmunol Neuroinflamm 2023;10;
DOI 10.1212/NXI.0000000000200141